Soft Matter

PAPER

View Article Online
View Journal | View Issue

Cite this: *Soft Matter*, 2014, **10**, 4990

Photo-activated ionic gelation of alginate hydrogel: real-time rheological monitoring of the two-step crosslinking mechanism†

Alina K. Higham,[a] Christopher A. Bonino,[a] Srinivasa R. Raghavan[b] and Saad A. Khan*[a]

We examine the gelation of alginate undergoing ionic crosslinking upon ultraviolet (UV) irradiation using *in situ* dynamic rheology. Hydrogels are formed by combining alginate with calcium carbonate ($CaCO_3$) particles and a photoacid generator (PAG). The PAG is photolyzed upon UV irradiation, resulting in the release of free calcium ions for ionic crosslinking. The viscous and elastic moduli during gelation are monitored as a function of the UV irradiation intensity, exposure time, alginate concentration, and the ratio between alginate and calcium carbonate. Gel time decreases as irradiation intensity increases because a larger concentration of PAG is photolyzed. Interestingly, dark curing, the continuing growth of microstructure in the absence of UV light, is observed. In some instances, the sample transitions from a solution to a gel during the dark curing phase. Additionally, when exposed to constant UV irradiation after the dark curing phase, samples reach the same plateau modulus as samples exposed to constant UV without dark curing, implying that dark curing does not affect the gelation mechanism. We believe the presence of dark curing is the result of the acidic environment persisting within the sample, allowing $CaCO_3$ to dissociate, thereby releasing free Ca^{2+} ions capable of binding with the available appropriate ionic blocks of the polymer chains. The growth of microstructure is then detected if the activation barrier has been crossed to release sufficient calcium ions. In this regard, we calculate a value of 30 J that represents the activation energy required to initiate gelation.

Received 20th February 2014
Accepted 12th May 2014

DOI: 10.1039/c4sm00411f

www.rsc.org/softmatter

Introduction

The fabrication of hydrogels from biocompatible materials is of interest since these malleable systems are excellent candidates for biomedical and tissue engineering applications.[1–4] Hydrogels are formed from polymer networks spanning in three dimensions and have the ability to swell in aqueous solutions. Additionally, the shape, mechanical stability, and rates of degradation can be tailored, making them promising materials for applications such as drug delivery and regenerative medicine.[5] As demands for less invasive procedures and smart materials grow, research focusing on the development of novel hydrogels has surged, specifically light responsive systems comprised of biocompatible materials.

Alginate, a polysaccharide derived from various species of brown algae, has been used extensively in applications such as tissue scaffolding,[6] the encapsulation and delivery of biological moieties (*i.e.*, cells, proteins, drugs),[2,7,8] wound healing,[9,10] and photopatterning to interface biological moieties with hard surfaces.[11–14] Alginate hydrogels are usually constructed *via* physical crosslinking mechanisms (ionic bonding with divalent cations such as Ca^{2+} and Mg^{2+}),[15,16] although chemical crosslinking is also possible (reaction with glutaraldehyde[17,18] or free-radical polymerization of methacrylated alginate[19,20]). Alginate hydrogels formed from these two mechanisms have shown promise; however, both possess inherent drawbacks, as chemical crosslinking requires the use of chemical reagents which present cytotoxicity concerns, while control over the gelation mechanism is difficult for typical physically crosslinked alginates.

Recently, the development of photoactivated alginate hydrogels has been reported to garner better control over alginate gelation. Photoactivated alginate hydrogels present benefits such as targeted, controlled, and minimally invasive gelation, which may be useful in biomedical or photopatterning applications, since light can be directed at a precise location from a distance, avoiding direct contact. To date current approaches for the fabrication of photoinitiated alginate hydrogels include: the synthesis of chemically modified alginate containing reactive methacrylate side groups,[21] the release of $CaCl_2$ from phototriggerable liposomes,[22] and the release of Ca^{2+} from photoresponsive Ca^{2+}chelators or cages.[23,24]

[a]*Department of Chemical and Biomolecular Engineering, North Carolina State University, Raleigh, NC 27695-7905, USA. E-mail: khan@eos.ncsu.edu; Tel: +1-919-515-4519*

[b]*Department of Chemical and Biomolecular Engineering, University of Maryland, College Park, MD 20742, USA*

† Electronic supplementary information (ESI) available. See DOI: 10.1039/c4sm00411f

Unfortunately, these alternate techniques require additional chemical synthesis steps or the use of expensive materials (caged Ca^{2+} and liposomes).

Javvaji *et al.*[21] have reported a novel system for the fabrication of photoactivated alginate hydrogels *via* physical crosslinking, based on the release of calcium ions from insoluble calcium carbonate ($CaCO_3$) nanoparticles. Their formulation employed inexpensive, commercial materials, *viz.* alginate, a photoacid generator (PAG) and $CaCO_3$ particles. Upon ultraviolet (UV) irradiation, the PAG was hydrolyzed, releasing acid (H^+). The release of acid triggered the solubilization of the $CaCO_3$ particles, releasing Ca^{2+} ions that combined with alginate to form the widely accepted "egg-box" junctions between alginate chains, creating a gel (Fig. 1).[25,26] Since the calcium ions and alginate form ionic bonds, the sample may be reversed into the sol state upon removal of the cation from the "egg-box" junction.

Alginate is comprised of β-D-mannuronate (M) and α-L-guluronate (G) residues which arrange in non-regular blockwise patterns along the linear chain. Residues can form three types of sequential blocks: alternating sequence (MG), repeat M residues (M-block), and repeat G residues (G-block). Paired G-sequences form a buckled structure in the shape of an "egg-box" whose cavity can accommodate divalent cations (*e.g.* Ca^{2+})

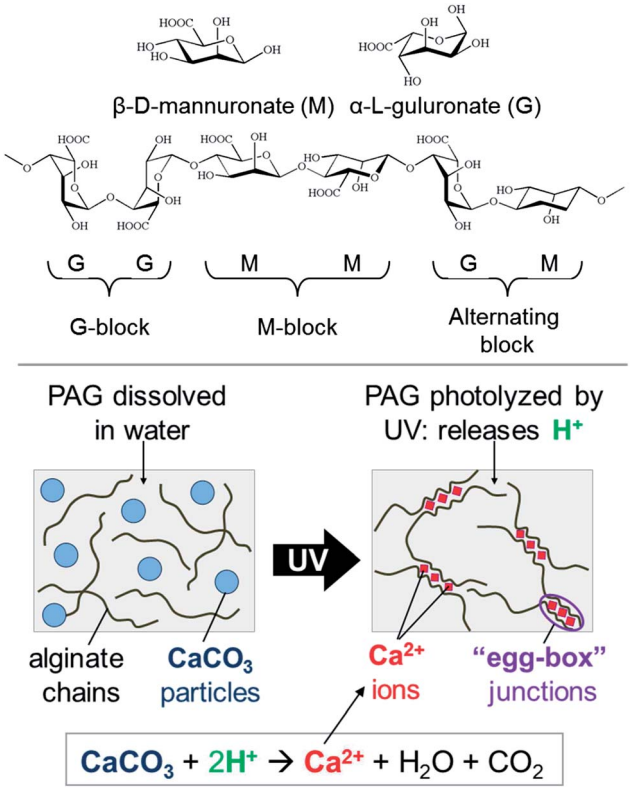

Fig. 1 Schematic and visual depiction of the UV initiated formation of an alginate hydrogel with the crosslinking procedure. The system consists of sodium alginate and a photoacid generator (PAG) dissolved in water with dispersed $CaCO_3$ particles. Note that G-blocks are comprised of sequential G-residues on the alginate backbone. Adapted from Javvaji *et al.*[21]

forming an ionic bond between G-blocks on adjacent alginate chains and the cation, schematic shown in Fig. 1.[27] As the sequence patterns and lengths of the varying blocks heavily depend on the biological source, alginate hydrogels may possess a wide range of gel properties, such as final modulus and crosslinking kinetics. An understanding of the relationship between the system components and time required for gelation would be beneficial for instances such as avoiding the irradiation of a sample for a longer duration of time than necessary.

Small-amplitude dynamic oscillatory rheology is an established technique for monitoring the gelation mechanism of crosslinking samples, as information regarding the magnitude of material properties such as the elastic (G') and viscous (G'') modulus can be attained without disrupting the fragile internal microstructure.[28–30] Rheological characterization of gelation mechanisms is critical for developing an understanding of the relationships between microstructure and product properties. Reported work[31–33] has focused solely on the rheological characterization of photoinitiated hydrogels undergoing chemical crosslinking mechanisms, the majority of which propagate *via* free-radical polymerization rather than physical gelation. Furthermore, most of these studies do not report *in situ* characterization of the gelation process, focusing only on characterization of the gelled samples.[21,34–36] Recently, *in situ* rheology under UV irradiation has been established to examine the kinetics of photocurable gels.[20,37–40] Such techniques are advantageous in that real-time quantitative information of the changing properties (G', G'') can be gathered as a function of time. Although rheological *in situ* characterization has been performed for the crosslinking of methacrylated alginate,[20] similar studies have not been performed for UV-activated physical crosslinking of alginate. In this study, we present a rheological study of UV-activated physically crosslinked alginate hydrogels, investigating the effects of UV intensity, irradiation exposure, and chemical composition on the gelation kinetics and final gel properties. We determine the relationship between gel point and UV intensity, as well as probe the role of the PAG in this crosslinking system. Other parameters investigated include the role of alginate concentration and the ratio of alginate and $CaCO_3$ concentration, as modulating the number of available G-blocks and/or Ca^{2+} ions will play a major role in the gel strength. We also examine the role of UV exposure time on final elastic modulus as dark curing is observed for this system. This phenomenon provides a means for tailoring the final gel properties by simply modulating UV exposure time without altering the sample composition.

Materials and methods

Materials

A model photoacid generator, diphenyliodonium nitrate, henceforth abbreviated as PAG, was used in our study. Both the PAG and sodium alginate (molecular weight: 12–40 kDa, originating from *Macrocystis pyrifera*) were purchased from Sigma Aldrich. Alginate originating from this specific source has been shown to have the following composition: alternating MG block 42%, M-block 40%, and G-block 18%.[41] Precipitated calcium

carbonate particles, mean particle radius of 70 nm, were obtained from Specialty Minerals from Birmingham, U.K.

Solution preparation and characterization

Solutions were prepared by mixing sodium alginate, PAG, and $CaCO_3$ particles in de-ionized water. Samples used in this study contain 4 wt/vol% alginate, 60 mM PAG, and 30 mM $CaCO_3$ unless otherwise stated. Mixtures were stirred by a magnetic stir bar at room temperature for approximately 6 hours until dissolved. Before use, samples were sonicated for 10 minutes. Stock solutions of 10 mL were prepared to enable multiple experiments.

The pH of the system was measured (accumet Basic AB15 pH meter) before, during, and after UV irradiation from a 200 W mercury lamp (Lumens Dynamic, Omnicure S2000, filter 320–500 nm) with a fiber glass optical light guide. Samples were gently stirred by a magnetic stir bar while irradiated to ensure homogeneity.

Rheological characterization

All rheology experiments were conducted using a stress-controlled Discovery Hybrid Rheometer HR-2 rheometer (TA Instruments) and 20 mm parallel plate geometry. Note that larger plate sizes are not commercially available because of problems associated with having UV light guide providing radially uniform intensity at larger diameters. All UV experiments were performed with the UV Light Guide accessory (TA Instruments) connected to a 200 W mercury arc bulb UV source (Lumens Dynamic, Omnicure S2000, filter 320–500 nm) with UV intensity equal to 175 mW cm^{-2}, unless otherwise stated. Solution gelling behavior was monitored using small amplitude dynamic oscillatory time and frequency sweeps, where time zero represents the start of UV irradiation. The stress applied to the sample was kept constant at 1 Pa, which was determined to be within the linear viscoelastic regime (LVR) by performing strain sweeps on the resultant gels.

Results and discussion

Evolution of crosslinking mechanism

As a starting point, the photogelling response of the system containing alginate, a photoacid generator (PAG), and calcium carbonate ($CaCO_3$) particles, was characterized before and after ultraviolet (UV) exposure using small amplitude dynamic oscillatory rheology, so as not to disturb the fragile developing microstructure. The frequency spectra can be seen in Fig. 2A. Sample behavior prior to irradiation shows typical solution characteristics. Both moduli have a strong dependence on frequency, while the magnitude of the viscous modulus, G'', is higher than the elastic modulus, G'. However, after 2000 s of UV exposure, the sample shows gel-like behavior, as G' is independent of frequency. Additionally, the magnitude of G' has increased by several orders of magnitude, surpassing G''. This change is indicative of the development of a complex microstructure, able to hold its own weight upon inversion as previously shown.[21] Upon UV irradiation, the PAG is photolyzed,

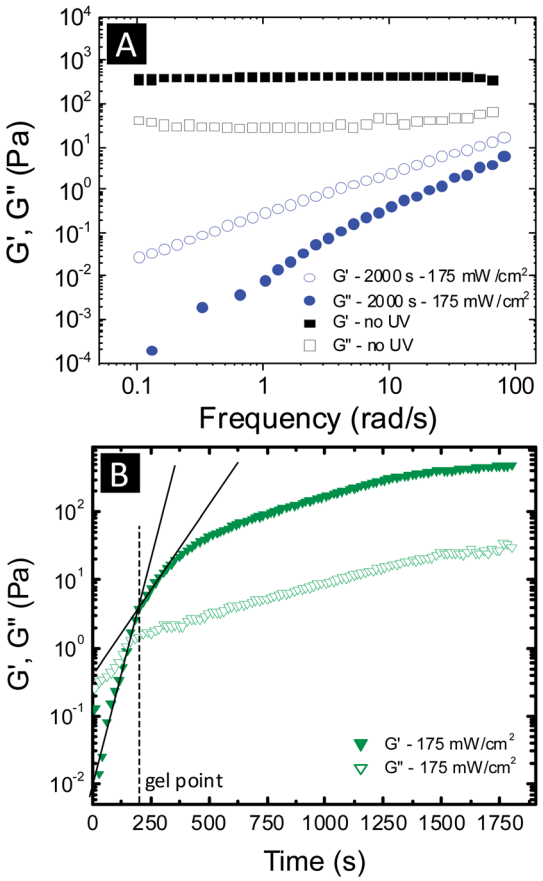

Fig. 2 (A) Frequency spectra of 4 wt/vol% alginate, 60 mM PAG, and 30 mM of $CaCO_3$ before and after UV irradiation. (B) Time sweep at 1 rad s^{-1} during constant UV irradiation. Lines are drawn to guide the eye in showing a change in slope during gelation.

releasing acid (H^+) into the system. The acid release triggers the dissociation of $CaCO_3$, releasing Ca^{2+} ions, which have been shown to ionically bond with consecutive α-L-guluronate (G) residues (G-blocks) along the alginate chain. The bonding of Ca^{2+} with G-blocks on adjacent alginate chains form "egg-box" junctions, resulting in a crosslinked network.[15,25,26]

In addition to characterizing samples before and after UV irradiation, we have monitored the transition from the sol state to the gelled state *in situ* during constant UV irradiation at a frequency of 1 rad s^{-1}, as shown in Fig. 2B. At time less than 200 s, the magnitude of G' is less than G'', with G' dramatically rising. Eventually, G' surpasses G'', with the G'–G'' crossover occurring at 150 s, and continues to grow, reaching a final value of 450 Pa. The initial sharp rise in G' can be attributed to the physical linking of Ca^{2+} ions with available G-blocks on adjacent alginate chains. Although G' continues to increase after the G'–G'' crossover, the rate of growth slows as demonstrated by a change in slope. Interestingly, the change in slope corresponds with the gel point, approximately 200 s (determination of which is explained in subsequent sections). This trend is also observed for samples exposed to varying UV intensities, shown later. Although gelation kinetics have been shown to slow over time for many gelation systems,[20,33] the change in slope

corresponding to the gel point seems to be unique to this system. We believe that this change in kinetics is due to diffusion limitations from the growing microstructure. Alginate chain mobility significantly decreases when free Ca^{2+} ions and available G-blocks from adjacent chains combine to form crosslinks. Free Ca^{2+} ions must diffuse through the developing microstructure to bond with unoccupied G-blocks, furthering microstructure growth. As the crosslinked network becomes more complex, the free Ca^{2+} ions have more barriers to diffusion, leading to a decrease in the rate of growth for G'. Further work in this aspect will be the focus of a future study.

Gel point determination

An important factor to consider when dealing with systems transforming from a solution to a gel is determination of the gel point (GP), the point in time at which the molecular weight of the system increases to infinity. Typically, gel points are rheologically detected using the Winter–Chambon criteria,[30,42–47] which states that at this juncture, G' and G'' are parallel to each other and have the same dependence on frequency. This can be graphically obtained by plotting tan δ (the ratio of G'' to G') *versus* time for varying frequencies, as depicted in Fig. 3A for a representative sample. We observe some scatter in the data and a maximum prior to the gel point, consistent with what has been reported for some systems in the literature.[20,37,40,48] However, the curves converge with time, with the point of intersection representing the gel point. In this case, the gel time corresponds to ~200 s. Tan δ time sweeps were performed at frequencies from 0.5 to 3 rad s^{-1}. This range allowed us to obtain the gel point using the Winter–Chambon criteria. Tan δ-time sweeps at higher frequencies ranges (above 3 rad s^{-1}) may refine the gel point value, but were limited in this study due to inertial effects inherent to small (2 cm) diameter top geometries. Advances in light-guide systems to accommodate larger top geometries (*e.g.*, 5 cm) will further improve this growing area of UV curing technologies.

Although the Winter–Chambon criteria is a well-established method for determining the gel point, it may require multiple experiments and it may occasionally be difficult to identify the point of intersection due to weak signals from G'' resulting in scattered data. Previously, our group reported the use of an empirical method for estimating the gel point for photo-initiated hydrogels comprised of chemically modified alginate by monitoring the percent strain over time.[20] While this approach has been demonstrated with alginate hydrogels, we are pursuing studies with other gel chemistries to ascertain the universality of this method. Monitoring the strain can be advantageous for systems with weak G'' signals after gelation or systems that experience rapid gelation, as both scenarios result in a narrow observation window for monitoring tan δ. When the sample approaches the gel point, the strain rapidly decreases as a result of the increasing modulus (Fig. 3B). The gel point can be estimated by a minimum in the derivative of the log strain with respect to time. We find that using both the Winter–Chambon criteria and the empirical approach reveal the same gel point for our system (200 s), indicating that the empirical approach works well for UV initiated alginate systems undergoing physical gelation, and may be used as an alternative method for quick gel point estimation.

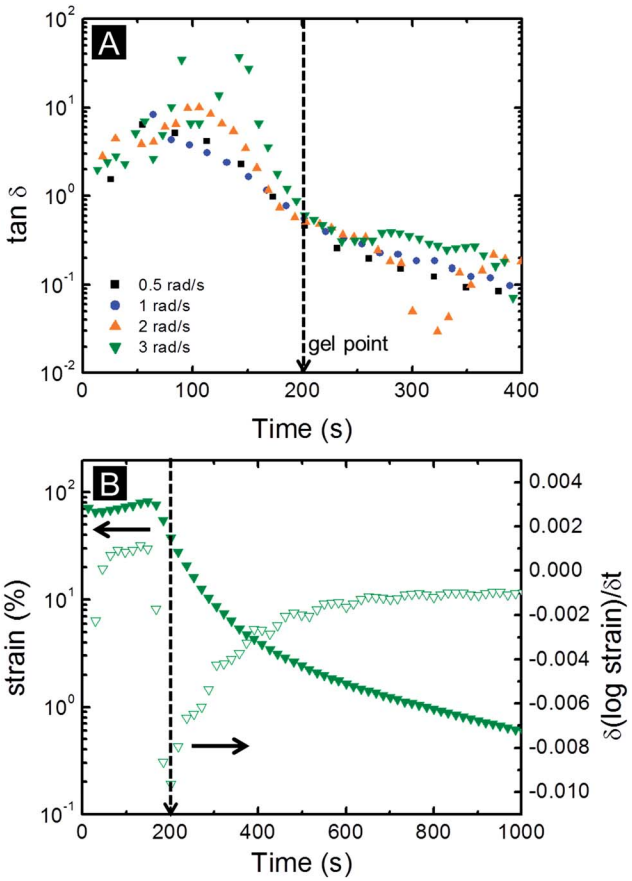

Fig. 3 (A) Loss tangent (tan δ) *versus* time for 4 wt/vol% alginate, 60 mM PAG, and 30 mM $CaCO_3$ at varying frequencies at constant UV irradiation of 175 mW cm^{-2}. The gel point corresponds to the intersection of the tan δ curves. (B) The gel point can also be determined by monitoring the sample strain over time at frequency of 1 rad s^{-1}. This occurs at the minimum of the derivative of strain with respect to time. Both methods match well.

Effect of UV intensity

It has been shown that gelation kinetics and final gel properties are directly affected by the UV intensity for photocurable systems.[20] We thus examined the evolution of our system from a solution to a gel over time for varying intensities and the corresponding frequency spectra of the final gels, as shown in Fig. 4. Note only data for G' is shown for clarity. Time sweeps containing both G' and G'' can be found in the ESI, Fig. S1.†

For all UV intensities investigated (75 mW cm^{-2} to 275 mW cm^{-2}), time sweeps show G' is initially lower than G'', but with continuing UV exposure, G' increases significantly, eventually surpassing G'', indicating the formation of an internal microstructure. Although the same general trend is seen for all samples, higher UV intensity shows an increase in the rate at which the microstructure grows (Fig. 4A inset). For instance, G' for a sample exposed to 275 mW cm^{-2} equals 80 Pa at 500 s,

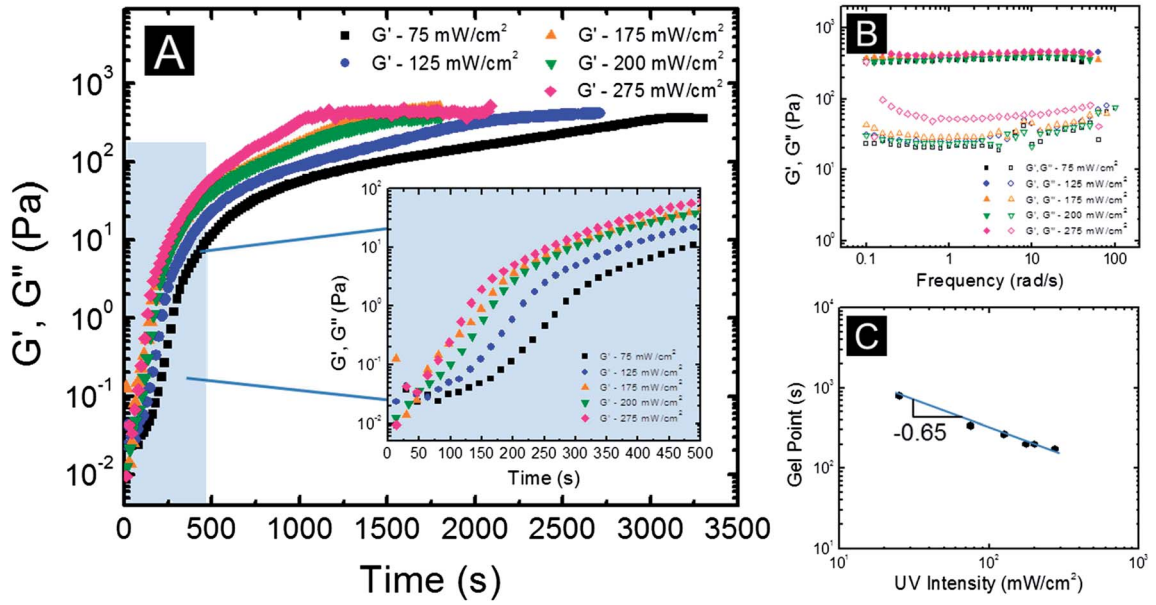

Fig. 4 (A) Time sweeps of 4 wt/vol% alginate, 60 mM PAG, and 30 mM $CaCO_3$ at varying UV intensities of 75 mW cm^{-2} to 275 mW cm^{-2}. (B) Frequency spectra of the final gels formed from irradiation at varying intensities. (C) Scaling of gel point with UV intensity.

while G' for a sample exposed to 75 mW cm^{-2} has only reached 10 Pa. The delay in gelation kinetics is also observed when pinpointing the gel point (GP), as determined by the previously discussed empirical method. We also observe that the gel point is inversely proportional to UV intensity (I), scaling as GP $\sim I^{-0.65}$ (Fig. 4C), a behavior consistent with previous results[20,38] although the exponent is different, possibly because of this having a different crosslinking (two-step ionic *versus* free radical) mechanism. Decreasing the UV intensity diminishes the amount of energy emitted from the UV source, providing less energy to enter the system in a specific period of time. This provides a delay in the release of acid from PAG, and subsequently, the release of Ca^{2+} for crosslinking. The microstructure develops more slowly due to fewer available Ca^{2+} ions for crosslinking and diffusional limitations due to the forming microstructure. Thus, a longer period of time is required before the gel point. It should be noted that although the gel point occurs after the G'–G'' crossover for all samples, this should not be unexpected. Systems possessing gel points that occur after the G'–G'' crossover are associated with large fractal dimensions (>2), representative of a closely packed system. Hydrogels formed by the physical crosslinking of alginate and calcium have been shown to create compact networks.[49]

Interestingly, despite the delay in gelation kinetics, all samples show G' plateaus at approximately the same magnitude given ample irradiation time. For instance, the plateau modulus for 275 mW cm^{-2} is reached at 1000 s, compared to 3000 s for 75 mW cm^{-2}. Frequency spectra of samples after UV irradiation show G' is independent of frequency and equal to the same magnitude (~400 Pa) for all gelled samples regardless of UV intensity (Fig. 4B). This is not what was observed in other physically crosslinked systems. For instance, gelatin crosslinking at higher temperature leads to a lower modulus due to the presence of fewer junction zones.[50] The authors attribute a "complex interplay of kinetics and thermodynamics" to explain their results. More importantly, similar final modulus was not observed for chemically crosslinked methacrylated-alginate, where the plateau modulus decreased as UV intensity was lowered due to a higher concentration of intramolecular crosslinks compared to intermolecular crosslinks.[20] For our physically crosslinking system, independence of the plateau modulus from UV intensity implies that the crosslinking mechanism is unaffected by UV intensity. The plateau modulus for this system is reached when all available G-blocks in the system have bonded with Ca^{2+} ions. Thus, the magnitude in plateau modulus is more likely dependent on the composition of the sample rather than intensity of UV exposure. For this photoinitiated alginate system, modulating the UV irradiation intensity alters the gelation kinetics without changing the crosslinking mechanism or final gel properties – thus the rate of formation may be tailored depending on the desired application without sacrificing final gel strength.

Varying UV exposure time and dark curing

Alginate hydrogels are beneficial for a variety of applications, requiring a wide range of final gel properties, especially gel modulus.[51] Since the gelation kinetics are dependent upon UV intensity during constant exposure, a means to modulate the final gel modulus may lie in altering the UV exposure time. We find that dark curing, defined as the continuing formation of an internal microstructure in the absence of UV light exposure, is prevalent for this system. Dark curing is not usually observed in most UV initiated systems that propagate *via* free radical polymerization, since radicals quickly self-terminate by recombination upon removal of UV irradiation. However, as our system does not propagate by free radical polymerization, we probed

the dark curing phenomenon further, identifying the effects of UV exposure time on the gelation and plateau modulus, as well as quantifying the dark curing effects.

The effects of dark curing are demonstrated for our system in Fig. 5A by monitoring G' and G'' over time after a specified duration of UV exposure at 175 mW cm^{-2} ranging from 20 s to 240 s. Note that G'' is not shown for clarity, but time sweeps containing G' and G'' can be found in the ESI (Fig. S2†). A single exposure of 20 s yields no change in G', even over 2500 s. Frequency spectra of the final sample after 20 s of UV irradiation show solution behavior as G'' is greater than G' and both moduli are frequency dependent (Fig. 5B). However, for exposure times greater than 20 s, an increase in G' is quickly detected, with both moduli increasing in magnitude over time after the removal of UV light. Dark curing from exposure times greater than 45 s yield completely gelled samples, as frequency spectra show G' independent of frequency (Fig. 5B). As expected, the rate of microstructure growth and the magnitude of the final gel modulus increase as the exposure times lengthen. Longer durations of exposure to UV irradiation allow more energy to enter the system, photolyzing a higher concentration of PAG and releasing a greater quantity of Ca^{2+} for crosslinking. The lack of change in microstructure after 20 s of UV exposure and the gelation of samples after UV exposure greater than 45 s infers that an activation energy must be reached in order to release ample H^+ to form a microstructure large enough for detection.

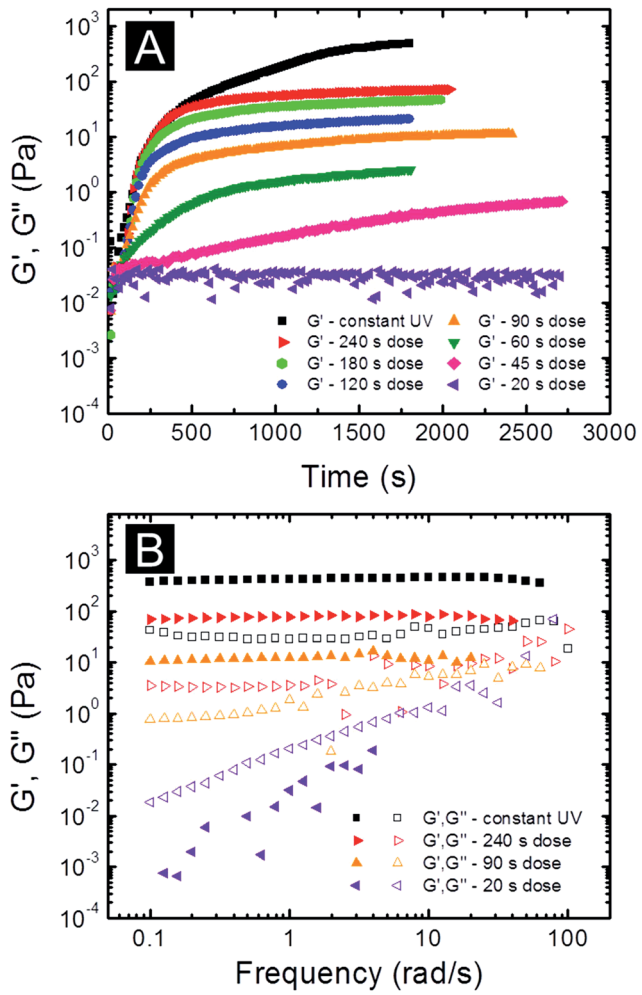

Fig. 5 (A) G' is monitored over time for samples of 4 wt/vol% alginate, 60 mM PAG, and 30 mM $CaCO_3$ after varying the duration of UV exposure from 20 seconds to 240 seconds, compared to continuous UV exposure at an intensity of 175 mW cm^{-2}. A minimum dosage time (*i.e.* activation energy) is required before any microstructure development is detected. (B) Frequency spectra for samples after dark curing phase for samples subjected to UV irradiation for 20 seconds, 90 seconds, 240 seconds, and continuous. Exposure duration of 20 seconds results in no change in microstructure, however, longer exposure times result in the sample transition from a solution to a gel during the dark curing phase.

In order to further probe this issue, we performed a single time sweep with multiple UV exposures of 20 s in duration (Fig. 6). After each UV exposure (presented by the shaded regions in the time sweep), G' and G'' were monitored over time in the absence of UV light, dividing the time sweep into four regions, each consisting of UV exposure, a dark curing phase, and corresponding frequency spectra. In region 1, the sample shows solution-like behavior and no change is observed for G' or G''. However, in region 2 (*i.e.* after the second UV exposure), G' is detectable and shown to grow over time during the dark curing phase. This demonstrates that the activation energy has been reached upon subsequent UV exposure and an adequate amount of Ca^{2+} ions are released to form a microstructure large enough for detection. It should be noted that the activation energy does not need to be reached by continuous UV exposure, but may be attained by discrete UV exposure steps. In region 3 (*i.e.* after the third UV exposure), G' surpasses G'' during the dark curing phase and frequency spectra of the sample after region 3 shows G' is greater than G'' and independent of frequency, indicative of a gelled sample. Note that the G'–G'' crossover, which is near the transition from a sol to gel, occurs in the absence of UV light, as shown in region 3 of Fig. 6. After the fourth 20 s dose, the microstructure continues to grow, with the magnitude of G' rising 4 Pa.

We believe the presence of dark curing is the result of a two-step crosslinking mechanism. When irradiated, UV energy is absorbed in the system, photolyzing the PAG and releasing H^+ ions. Although the UV sample is no longer exposed to UV light, the acidic environment within the sample persists, allowing $CaCO_3$ to dissociate, thereby releasing free Ca^{2+} ions capable of binding with available G-blocks. The growth of microstructure is then detected if the activation barrier has been crossed (sufficient Ca^{2+} ions have been released). Additionally, dark curing could also be a result of the time required for Ca^{2+} ions to diffuse towards available G-blocks. The continuation of gelation is therefore dependent on the presence of acid and Ca^{2+} ions, not the constant exposure to UV light as is the case for most crosslinking systems. This hypothesis was confirmed by monitoring the pH of the system before, during, and after timed exposures to UV light (Fig. 7C). During UV exposure, the pH drops from an initial value of 8 to 6.5 as a result of the release of acid from the photolyzed PAG. However, after UV irradiation is removed, the pH remains unchanged for a few minutes

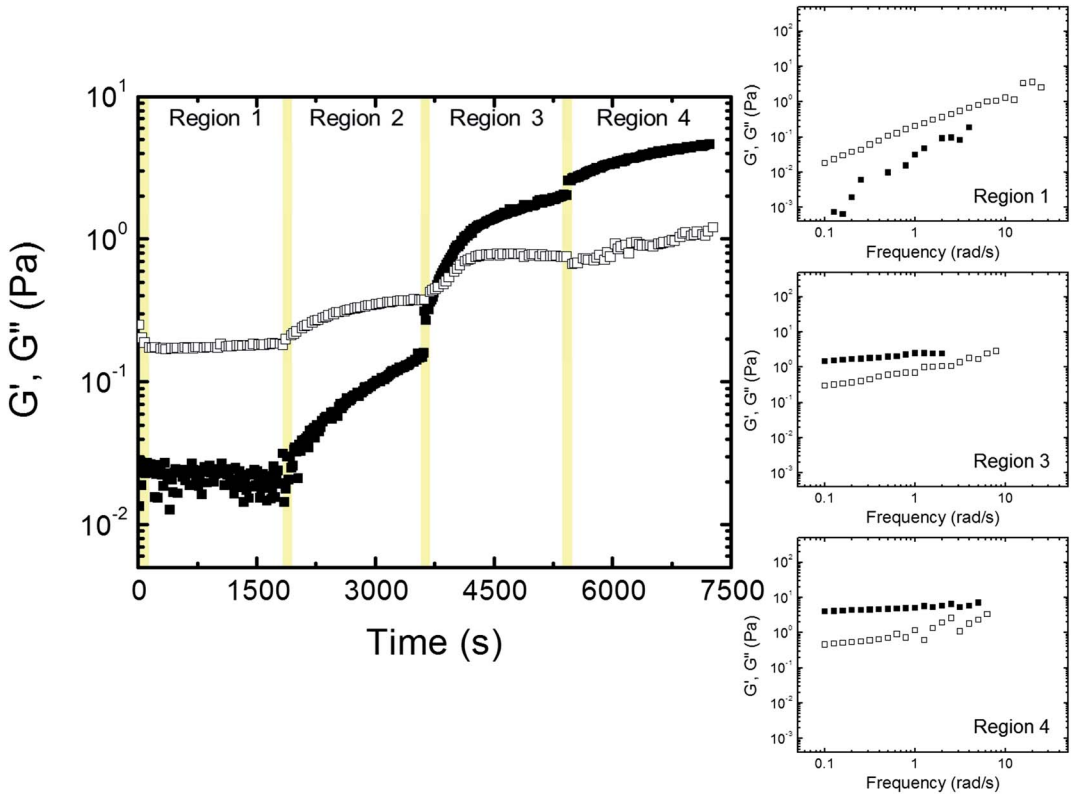

Fig. 6 Time sweep for 4 wt/vol% alginate, 60 mM PAG, and 30 mM $CaCO_3$ subjected to four 20 second doses of UV irradiation at 175 mW cm^{-2}, indicated by the shaded areas. G' and G'' were monitored during and after UV exposure. Frequency spectra (right hand plots) show the sample is in the solution state after region 1. However, the sample transitions from a solution to a gel during the dark curing phase in region 3. Subsequent exposure to UV causes further microstructure growth, as G' increased in magnitude (region 4).

demonstrating a persistent acidic environment in the absence of UV light. The pH then slowly increases as the acid is consumed in the dissociation reaction of $CaCO_3$ particles, creating Ca^{2+} ions and CO_2. It is interesting to note that the pH after UV exposure plateaus at a pH value lower than the initial solution prior to UV exposure, most likely due to the consumption and resulting decrease in concentration of $CaCO_3$ particles, whose presence creates a more basic environment (higher pH). This trend persisted for subsequent exposures to UV irradiation. Since exposure to UV light quickly photolyzes PAG and drops the pH, we can infer that dark curing is due to the dissociation of $CaCO_3$ and the diffusion of free Ca^{2+} ions to available G-blocks, even after UV irradiation is removed.

While understanding the mechanism responsible for dark curing in this system is important, it is also necessary to quantify the dark curing effects. Samples exposed to UV irradiation for a varying duration of time show a plateau in the magnitude of G' after the dark curing phase. This plateau in G' possibly relates to the incorporation of all Ca^{2+} ions freed during initial UV exposure into the microstructure. Since the magnitude of the plateau modulus relates to UV exposure time, the following equation is used to quantify the dark curing effects:

$$\text{Extent of dark curing} = \frac{G'_{\text{final}} - G'_{t=\text{UV off}}}{G'_{t=\text{UV off}}} \quad (1)$$

where G'_{final} represents the magnitude of the elastic modulus when plateaued at the end of dark curing, and $G'_{t=\text{UV off}}$ represents the magnitude of G' at the end of UV exposure.

A plot of the extent of dark curing as a function of UV exposure duration can be seen in Fig. 7A for our system. As stated previously, UV exposure of 20 s was not long enough to initiate the formation of a detectable microstructure, thus there is a lack of dark curing. As the UV exposure time increases from 45 s to 90 s, the change in magnitude of G' (*i.e.*, extent of dark curing) grows from 40 times $G'_{t=\text{UV off}}$ to 162 times $G'_{t=\text{UV off}}$ during the dark curing phase. As more energy is added into the system *via* longer exposure times, a larger concentration of PAG is photolyzed, thereby allowing for the dissociation of a larger quantity of $CaCO_3$ particles and thus free Ca^{2+} ions available for crosslinking. However, a maximum in the extent of dark curing is seen to occur around 90 s, even though the magnitude of G'_{final} continues to increase with lengthened UV exposure time. At UV exposure times greater than 90 s, microstructure formation occurs during the initial exposure, thus increasing the value of $G'_{t=\text{UV off}}$. Many of the Ca^{2+} ions are released during UV exposure and bond with available G-blocks before the UV light is removed. Thus, the extent of dark curing decreases for prolonged exposure times as the microstructure grows minimally after the removal of UV light.

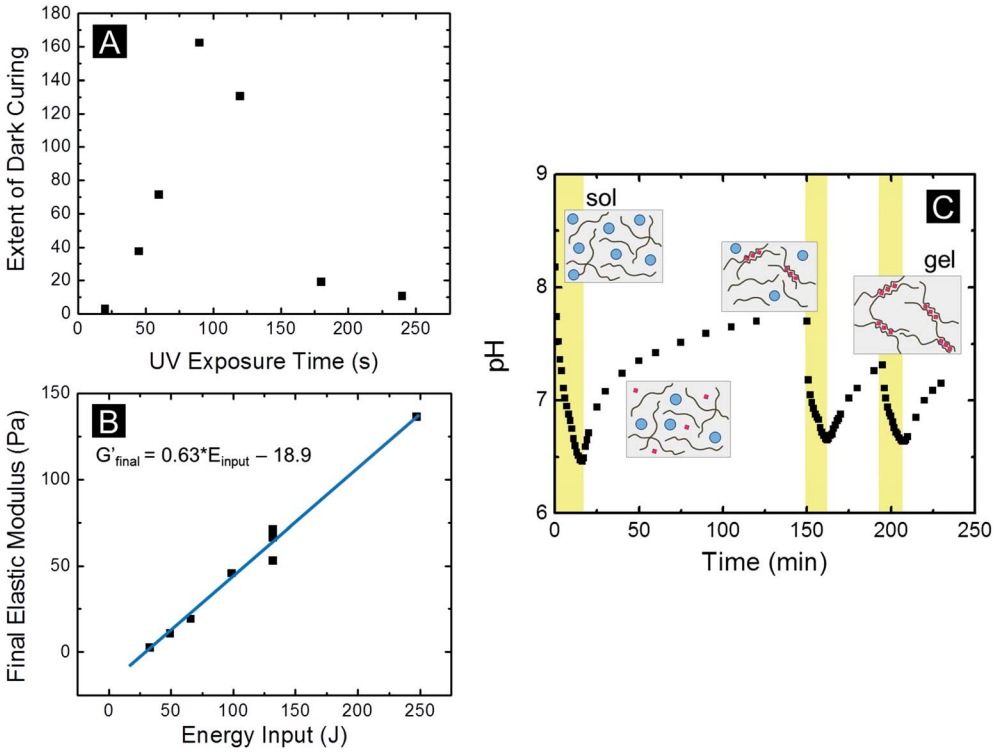

Fig. 7 (A) The extent of dark curing is shown as a function of UV exposure time for 4 wt/vol% alginate, 60 mM PAG, and 30 mM $CaCO_3$ at UV intensity of 175 mW cm^{-2}. (B) G' after the dark curing phase is shown as a function of energy input. (C) Monitoring of pH as a function of time during and following UV irradiation. Schematic images depict the two-step crosslinking mechanism during the dark curing phase.

As mentioned previously, the magnitude of G'_{final} increases as exposure time is lengthened, inferring that there is a relationship between G'_{final} and UV exposure time. Plotting G'_{final} as a function of energy input E_{input}, which is the product of power and time, shows a linear trend modeled by an empirical mathematical equation (Fig. 7B). It should be noted that this equation yields an x-intercept value of 30 J. This value represents the activation energy required to release ample Ca^{2+} ions to form a microstructure large enough for detection. The relationship between G'_{final} and energy input can be used to predict and tailor the final magnitude of G' for a sample by simply modulating the duration of UV exposure without having to alter the sample composition.

Another factor to consider is whether the energy input has a direct effect on the crosslinking kinetics. The phenomenon of reciprocity, whether the final modulus is dependent upon the UV exposure procedure, is investigated by performing rheological experiments where UV intensity and exposure times are varied, while maintaining an equivalent energy input. Two scenarios exist where the energy input is maintained. One scenario varies the UV exposure procedure for constant UV intensity (*e.g.* 120 s dose at 175 mW cm^{-2}, a 90 s and subsequent 30 s dose, or two doses each lasting 60 s in duration). Time sweeps monitoring G' and G'' during these UV exposure procedures can be found in Fig. 8A, with corresponding frequency spectra in Fig. 8C. At the end of each experiment, the total energy emitted equals 66 J. It is interesting to note that initial doses of 120, 90, and 60 s emit ample energy for the sample to transition from a solution to a gel during the dark curing phase; however, microstructure growth is not detected until the second dose when emitting in 20 s increments (shown previously). This can be attributed to the fact that a dose of 20 s at 175 mW cm^{-2} equals an energy input of 11 J, which is less than the calculated activation energy of 30 J. Thus, an inadequate amount of Ca^{2+} ions to form a microstructure large enough for detection have released. We find the magnitude of G' after dark curing for each sample is equal, suggesting that the mechanism for crosslinking remains unaffected by UV exposure procedure and that reciprocity is maintained when comparing samples irradiated with the same intensity. The second scenario for maintaining equal energy input is by altering both the intensity and the dosage time during continuous UV exposure. Our system was exposed to UV intensities ranging from 75 mW cm^{-2} to 175 mW cm^{-2} for varying exposure times, while maintaining a total energy input of 133 J. The samples were characterized *via* time sweeps and frequency sweeps of the resultant gel, Fig. 8B and D, respectively. A delay in the gelation kinetics is seen when the UV intensity decreases and microstructure growth occurs in the absence of UV light as a result of dark curing, as was previously discussed. After ample time has elapsed, G' is shown to plateau as all free Ca^{2+} released during UV exposure have bonded with G-blocks on the alginate chains. Interestingly, frequency spectra of the resultant gels show the magnitude of G' to be similar for all experiments of energy input 133 J, showing that reciprocity is also maintained when modulating both UV intensity and exposure time. Knowledge of

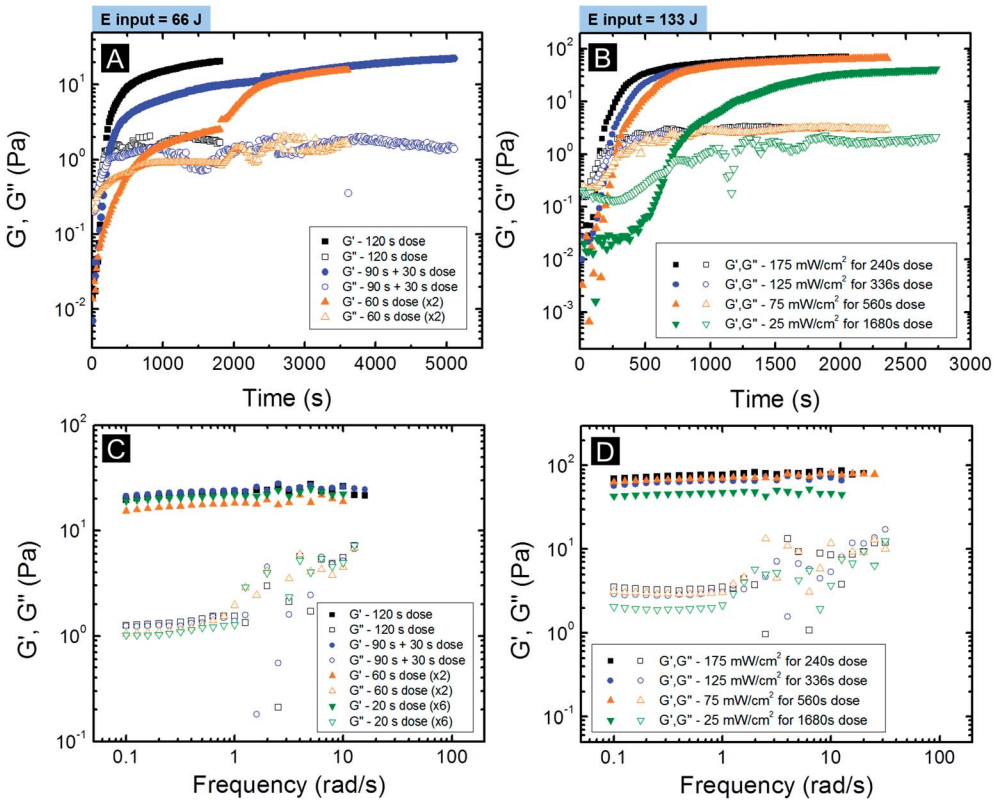

Fig. 8 Time sweeps and corresponding frequency spectra of 4 wt/vol% alginate, 60 mM PAG, and 30 mM $CaCO_3$ for energy inputs of (A and C) 66 Joules and (B and D) 133 Joules. Data shows reciprocity is exhibited by this system for durations of UV exposure shorter and longer than the gel point.

this phenomenon is advantageous in predicting processing procedures for the formation of gels with equal moduli despite variation in UV intensity from different UV sources. Reciprocity, in combination with the relationship between final gel modulus and energy input discussed previously, provide a means to tailor the final modulus by modulating the energy input, independent of UV intensity.

One important factor to note is that the crosslinking mechanism, driven by the formation of egg-box junctions, remains unaffected during the dark curing phase, as illustrated in Fig. 9. A representative system is first exposed to UV irradiation for 180 s and then monitored during the dark curing phase for 2000 s, as shown in Fig. 9A in region 1. During the dark curing phase, the magnitude of G' increases to 45 Pa. Upon subsequent exposure to constant UV irradiation after the dark curing phase (time of 2000 to 4000 s, region 2), G' is shown to increase, eventually reaching the magnitude of 400 Pa which seems to be equal to the plateau modulus for a sample exposed to continuous UV irradiation (Fig. 9A). In Fig. 9B, we show the frequency spectra for a sample from region 1 (after 180 s of UV exposure and the dark curing phase), region 2 (after 180 s of UV exposure, dark curing, and subsequent constant UV irradiation), and a sample exposed to continuous UV irradiation with no dark curing phase. The magnitudes of G' and G'' of the sample from region 1 increase upon subsequent constant UV exposure (region 2). Additionally, the frequency spectra from region 2 show both dynamic moduli to be equal to that for a sample exposed to continuous UV irradiation with no dark curing phase. This effect is also shown for samples exposed to constant UV irradiation after exposure times of 240 s and 450 s and their respective dark curing phases (Fig. 9C). After exposure to constant UV irradiation, all samples show a final modulus of 400 Pa. This equality infers that the crosslinking mechanism during the dark curing phase is the same mechanism used to form a microstructure under constant irradiation. The ability to pause at a specific magnitude of G' and subsequently continue microstructure growth upon additional UV irradiation may prove to be beneficial for applications where varying moduli are required at specific times.

Composition effects

Although processing effects are important to investigate, it is also imperative to understand the relationship between sample composition and properties of the resultant gel. One such factor is the ratio of G-blocks in the alginate chain to the number of available Ca^{2+} ions. The theoretical maximum amount of calcium ions the system is able to accommodate (henceforth referred to as the theoretical maximum) can be calculated by assuming a 2 : 1 G-block to Ca^{2+} ion ratio (from one "egg-box" junction) and using the reported composition percentage of alginate derived from *Macrocystis pyrifera* (42% alternating MG-block, 40% M-block, and 18% G-block).[41] Time sweeps and

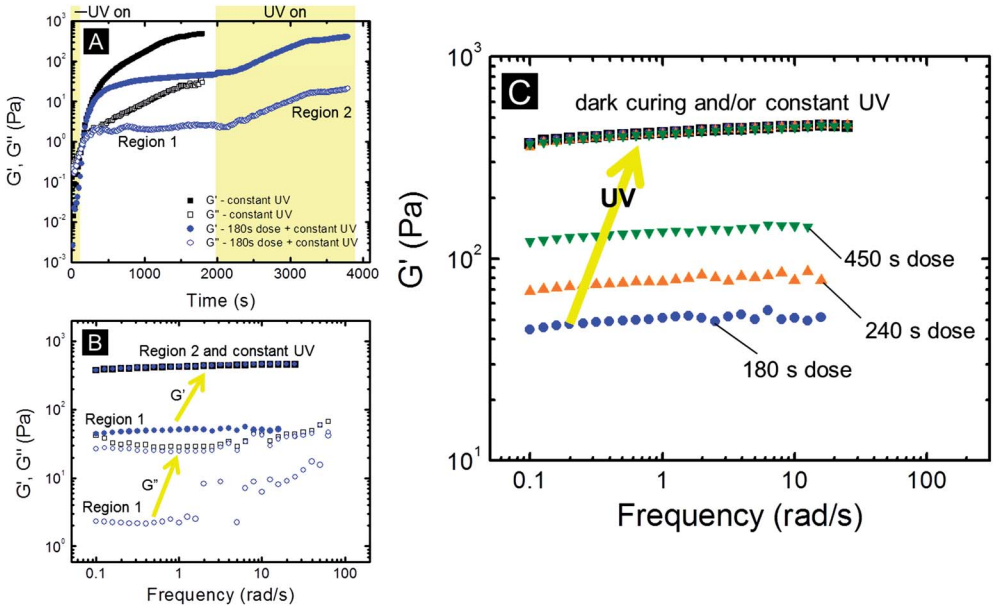

Fig. 9 (A) Time sweep and (B) frequency spectra of 4 wt/vol% alginate, 60 mM PAG, and 30 mM $CaCO_3$ exposed to UV irradiation at 175 mW cm^{-2} for 180 seconds and then subsequent continuous UV exposure, shown by the shaded regions. After the dark curing phase, the sample exhibits gel-like behavior. After additional UV exposure, G' increases to a magnitude equal to the final modulus of a gel exposed to constant UV irradiation. (C) Frequency spectra showing the magnitude of G' for a gel exposed to constant UV irradiation can be obtained with continuous UV exposure after short durations of UV exposure for 180, 240, and 450 seconds.

frequency sweeps of irradiated samples containing concentrations of $CaCO_3$ varying from 0.25 times the theoretical maximum to 1.5 times the theoretical maximum can be found in Fig. 10A and B, respectively. Time sweeps containing G'' are not shown for clarity, but can be found in the ESI (Fig. S3†). It should be noted that the alginate concentration (4 wt/vol%) and the ratio of PAG to $CaCO_3$ of 2 : 1 remained constant. As expected, samples containing 0.25 and 0.5 times the theoretical maximum are unable to form microstructures large enough for detection, as an insufficient amount of calcium is available. Frequency spectra of these systems after 2800 s of UV irradiation (Fig. 10B) show solution behavior as G' is heavily dependent on frequency. However, as the amount of calcium is increased to 0.75 times the theoretical maximum, the solution shows microstructure growth upon irradiation with G' increasing to a value of 50 Pa. As the concentration of $CaCO_3$ is further increased to the theoretical maximum and 1.5 times the theoretical maximum, samples show faster microstructure growth as the plateau modulus is reached in a shorter period of time. Samples containing increasing concentrations of $CaCO_3$ are able to reach the plateau modulus more quickly as a larger amount of calcium ions are available for crosslinking, which reduces the amount of time required for the ions to diffuse through the microstructure and find available G-blocks. Frequency spectra of samples containing greater than 0.5 times the theoretical maximum show gel behavior as G' is independent of frequency and of magnitude greater than G'' (Fig. 10B) implying that a minimum quantity of crosslinks, and thus available Ca^{2+} ions, is required for the formation of any detectable microstructure. Increasing the number of crosslinks produces stronger gels, as G' increases from 50 Pa to 400 Pa when the concentration of $CaCO_3$ is raised from 0.75 times the theoretical maximum to 1.5 times the theoretical maximum. An increase in the concentration of $CaCO_3$, and thus available Ca^{2+} ions, allows for more crosslinks between G-blocks on adjacent alginate chains to form, creating stronger microstructures with a larger G'. Interestingly, samples containing the theoretical maximum and 1.5 times the theoretical maximum have equal plateau moduli (400 Pa). The final modulus remains unaffected since all of the available G-blocks on the alginate chain are occupied by calcium ions, despite there being excess Ca^{2+}. Although gelation kinetics and gel strength are improved with excess $CaCO_3$, the maximum gel modulus remains unaffected, as this value is determined by the quantity of G-blocks in the system when calcium is in excess. These findings are consistent with previous studies stating that the gel strength is directly related to the fraction of G-blocks within the sample.[52] However, Morris and co-workers have found the gel modulus of gellan gum to show a maximum with continuing increase in ionic strength.[53] They attributed this behavior to the formation of non-homogeneity in microstructure at high cationic concentrations. Since the cationic concentration in our system (45 mM) is considerably smaller than the range used in the previous study, it remains to be seen if we would observe a similar decrease in modulus at much higher cationic concentrations.

Additionally, the concentration of alginate can be modulated while maintaining the calcium concentration to be 1.5 times the theoretical maximum. It must be noted that the theoretical maximum amount of calcium was adjusted for each sample, since this value depends upon the quantity of G-blocks which is directly affected by the concentration of alginate. A minimum alginate concentration is required for the formation of a

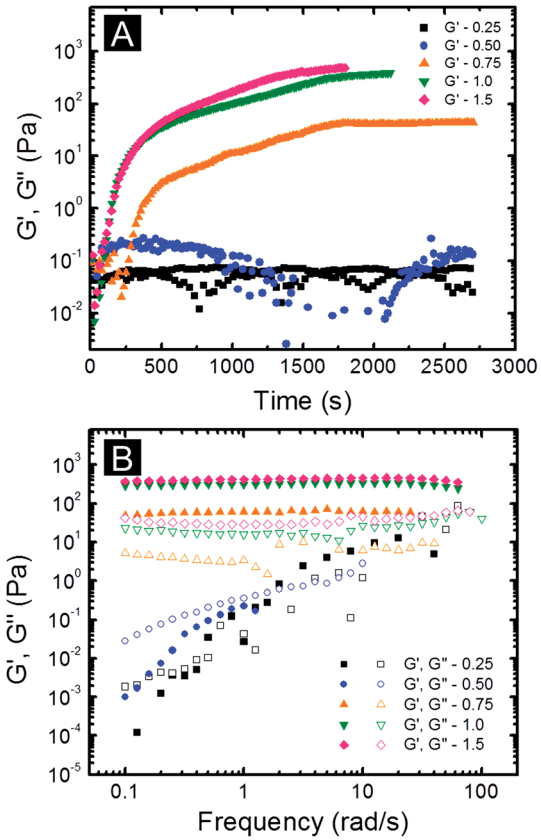

Fig. 10 (A) Time sweeps and (B) frequency spectra of 4 wt/vol% alginate with varying concentrations of $CaCO_3$, ranging from 0.25 to 1.5 times the maximum theoretical amount. Concentrations greater than 0.5 times the theoretical maximum are required to form an internal microstructure, since lower ratios do not contain enough calcium to create an adequate number of crosslinks. Frequency spectra shows samples containing 0.25 and 0.5 times the theoretical maximum result in solution behavior as G' and G'' are dependent upon frequency. Samples containing 1 and 1.5 times the theoretical maximum show equal magnitudes of G', indicating the gel strength is greatly dependent on quantity of available G-blocks when calcium is in excess.

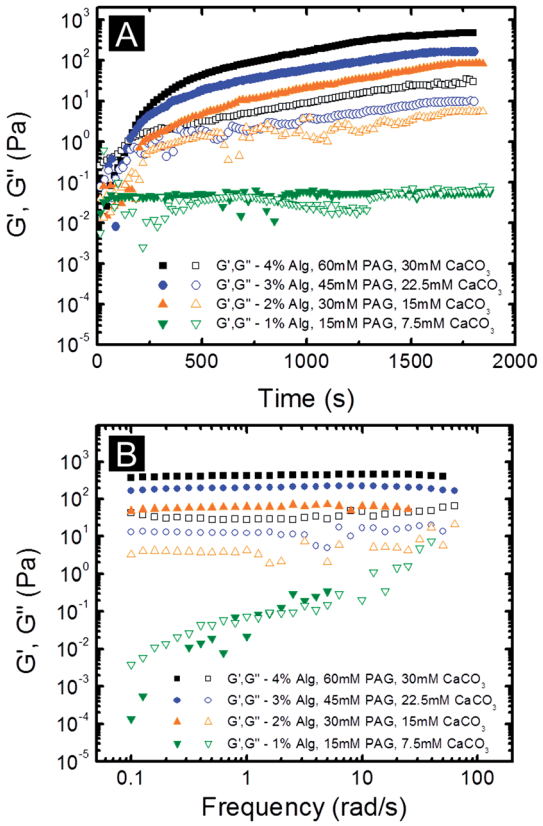

Fig. 11 (A) Time sweeps and (B) frequency spectra of samples containing varying concentrations of alginate, while maintaining a calcium concentration of 1.5 times the maximum theoretical amount, subjected to UV irradiation of 175 mW cm^{-2}. 1 wt/vol% alginate contains too few G-blocks to create a microstructure, while increasing concentration results in stronger gels.

microstructure large enough for detection as time sweeps of systems containing 1 wt/vol% alginate during constant UV irradiation show no change in G' (Fig. 11A). Frequency spectra after 1800 s of UV irradiation for this system show solution behavior as G' and G'' are dependent upon frequency (Fig. 11B). Time sweeps of samples containing alginate concentrations ranging from 2 to 4 wt/vol% during constant UV irradiation show growth in G' over time, indicating the formation of an internal microstructure. The magnitude of the final gel modulus, depicted *via* frequency spectra (Fig. 11B), increases with the concentration of alginate. In particular, the final modulus shows a power-law behavior with respect to concentration, *i.e.*, $G' \sim (C - C_o)^n$ with the power-law exponent $n = 2$ in our case. Such behavior with concentration dependence larger than unity is akin to what has been observed in other physically cross-linked systems.[50] Increasing the alginate concentration introduces a higher quantity of G-blocks, which presents a larger number of potential crosslinking sites, creating an intricate and stronger microstructure. This provides another means of altering the final gel properties dependent upon the desired magnitude of G' which is usually application dependent.

Conclusions

We have performed an *in situ* rheological study during the UV-activated gelation of alginate. UV irradiation is used to photolyze a PAG, which releases acid causing the dissolution of dispersed $CaCO_3$ particles and liberation of free Ca^{2+} ions to form egg-box junctions with adjacent alginate chains. Gel points for a system of 4 wt/vol% alginate with 60 mM PAG and 30 mM $CaCO_3$ were determined using an empirical approach that monitors strain over time and was shown to correlate well with the Winter–Chambon criterion for gel point. The time required for gelation decreased as the UV intensity increases, because a higher UV intensity photolyzes a larger fraction of PAG molecules, thus releasing a larger concentration of Ca^{2+} ions. Most interestingly, evidence of microstructure growth in the absence of UV light, also known as dark curing, was observed. For our system irradiated at an intensity of 175 mW cm^{-2}, the extent of dark curing increases with UV exposure time

up to 90 s. Dark curing indicates a two-step crosslinking mechanism, specifically the time required for Ca^{2+} to diffuse to available G-blocks and a persistent acidic environment which allows for the release of Ca^{2+} ions in the absence of UV light. The crosslinking mechanism remains unaffected by dark curing, as samples exposed to UV irradiation for a short period of time and then subsequent continuous UV irradiation produce gels with the same modulus as a sample continuously exposed to constant UV irradiation. The final elastic modulus can be predicted by the energy input, providing a means to tailor samples by modulating the duration of UV exposure and irradiation intensity. Lastly, the effects of composition such as alginate concentration and the ratio of alginate and $CaCO_3$ on gelation kinetics and final gel modulus were investigated. A minimum concentration of calcium (0.5 times the theoretical maximum) and alginate (2 wt/vol%) were both required for the formation of gels. Increases in $CaCO_3$ and alginate concentrations enhance the gelation kinetics and gel strength. Interestingly, the final elastic modulus is dependent upon the quantity of G-blocks since the final elastic modulus remains unchanged when the $CaCO_3$ concentration is greater than the theoretical maximum. In this case, once all available G-blocks have bonded with Ca^{2+} ions, excess calcium ions are unable to form any further crosslinks. Additionally, the final gel modulus increases as the alginate concentration increases since the quantity of G-blocks available for crosslinking has increased. Overall, this system provides a means for fabricating alginate hydrogels upon UV irradiation, but specifically, the dark curing phenomenon provides a means to tailor the final elastic modulus by modulating the energy input into the system without having to alter the gel composition. This alginate hydrogel system would be suitable in a plethora of applications as a wide range of elastic moduli magnitudes are easily attained by simply modulating composition and processing parameters.

Acknowledgements

The authors would like to thank Russell Turner at Lumens Dynamics for the UV source, Sarah Cotts, Steve Aubuchon, and the rheology department at TA Instruments in New Castle, DE for the *in situ* UV rheometer accessory. We would also like to thank Esther Lee and Andrew Kessler for their hard work and help in laying the foundation for this project, and Nancy Burns for her help with this research project.

References

1 K. Anseth, C. Bowman and L. BrannonPeppas, *Biomaterials*, 1996, **17**, 1647–1657.
2 S. Bryant, C. Nuttelman and K. Anseth, *J. Biomater. Sci., Polym. Ed.*, 2000, **11**, 439–457.
3 J. Burdick, A. Peterson and K. Anseth, *Biomaterials*, 2001, **22**, 1779–1786.
4 M. Freeman, M. Furey, B. Love and J. Hampton, *Wear*, 2000, **241**, 129–135.
5 J. Jagur-Grodzinski, *Polym. Adv. Technol.*, 2010, **21**, 27–47.
6 C. K. Kuo and P. X. Ma, *Biomaterials*, 2001, **22**, 511–521.
7 M. F. A. Goosen, G. M. Oshea, H. M. Gharapetian, S. Chou and A. M. Sun, *Biotechnol. Bioeng.*, 1985, **27**, 146–150.
8 W. R. Gombotz and S. F. Wee, *Adv. Drug Delivery Rev.*, 1998, **31**, 267–285.
9 A. D. Augst, H. J. Kong and D. J. Mooney, *Macromol. Biosci.*, 2006, **6**, 623–633.
10 B. Balakrishnan, M. Mohanty, P. R. Umashankar and A. Jayakrishnan, *Biomaterials*, 2005, **26**, 6335–6342.
11 X. Shi, C. Tsao, X. Yang, Y. Liu, P. Dykstra, G. W. Rubloff, R. Ghodssi, W. E. Bentley and G. F. Payne, *Adv. Funct. Mater.*, 2009, **19**, 2074–2080.
12 S. A. Zawko and C. E. Schmidt, *Lab Chip*, 2010, **10**, 379–383.
13 P. J. Bracher, M. Gupta and G. M. Whitesides, *Adv. Mater.*, 2009, **21**, 445–450.
14 P. J. Bracher, M. Gupta, E. T. Mack and G. M. Whitesides, *ACS Appl. Mater. Interfaces*, 2009, **1**, 1807–1812.
15 Y. Fang, S. Al-Assaf, G. O. Phillips, K. Nishinari, T. Funami and P. A. Williams, *Carbohydr. Polym.*, 2008, **72**, 334–341.
16 Y. Fang, S. Al-Assaf, G. O. Phillips, K. Nishinari, T. Funami, P. A. Williams and L. Li, *J. Phys. Chem. B*, 2007, **111**, 2456–2462.
17 H. Kong, D. Kaigler, K. Kim and D. Mooney, *Biomacromolecules*, 2004, **5**, 1720–1727.
18 C. Yeom and K. Lee, *J. Appl. Polym. Sci.*, 1998, **69**, 1607–1619.
19 O. Jeon, K. H. Bouhadir, J. M. Mansour and E. Alsberg, *Biomaterials*, 2009, **30**, 2724–2734.
20 C. A. Bonino, J. E. Samorezov, O. Jeon, E. Alsberg and S. A. Khan, *Soft Matter*, 2011, **7**, 11510–11517.
21 V. Javvaji, A. G. Baradwaj, G. F. Payne and S. R. Raghavan, *Langmuir*, 2011, **27**, 12591–12596.
22 Z. Zhang, P. Shum, M. Yates, P. Messersmith and D. Thompson, *Bioconjugate Chem.*, 2002, **13**, 640–646.
23 J. Cui, M. Wang, Y. Zheng, G. M. R. Muniz and A. del Campo, *Biomacromolecules*, 2013, **14**, 1251–1256.
24 B. Chueh, Y. Zheng, Y. Torisawa, A. Y. Hsiao, C. Ge, S. Hsiong, N. Huebsch, R. Franceschi, D. J. Mooney and S. Takayama, *Biomed. Microdevices*, 2010, **12**, 145–151.
25 P. Sikorski, F. Mo, G. Skjak-Braek and B. T. Stokke, *Biomacromolecules*, 2007, **8**, 2098–2103.
26 Y. Fang, S. Al-Assaf, G. O. Phillips, K. Nishinari, T. Funami, P. A. Williams and L. Li, *J. Phys. Chem. B*, 2007, **111**, 2456–2462.
27 I. Braccini and S. Perez, *Biomacromolecules*, 2001, **2**, 1089–1096.
28 G. Odian, in *Principles of Polymerization*, ed. anonymous, John Wiley & Sons, New York, 1991, pp. 103–104–112.
29 C. W. Macosko, *Rheology Principles, Measurements, and Applications*, Wiley-VCH, New York, 1994.
30 H. H. Winter, in *Encyclopedia of Materials: Science and Technology*, ed. K. H. J. Buschow, R. W. Cahn, M. W. Flemings, B. Ilschner, E. J. Kramer and S. Mahajan, Elsevier, New York, 2001, pp. 6991–6999.
31 S. Khetan and J. A. Burdick, *Biomaterials*, 2010, **31**, 8228–8234.
32 B. D. Fairbanks, M. P. Schwartz, A. E. Halevi, C. R. Nuttelman, C. N. Bowman and K. S. Anseth, *Adv. Mater.*, 2009, **21**, 5005–5010.

33 C. N. Bowman and C. J. Kloxin, *AIChE J.*, 2008, **54**, 2775–2795.
34 T. Matsumoto and K. Mashiko, *Biopolymers*, 1990, **29**, 1707–1713.
35 B. T. Stokke, K. I. Draget, O. Smidsrød, Y. Yuguchi, H. Urakawa and K. Kajiwara, *Macromolecules*, 2000, **33**, 1853–1863.
36 X. Liu, L. Qian, T. Shu and Z. Tong, *Polymer*, 2003, **44**, 407–412.
37 B. Chiou, S. Raghavan and S. Khan, *Macromolecules*, 2001, **34**, 4526–4533.
38 S. Khan, I. Plitz and R. Frantz, *Rheol. Acta*, 1992, **31**, 151–160.
39 B. Chiou and S. Khan, *Macromolecules*, 1997, **30**, 7322–7328.
40 B. Chiou, R. English and S. Khan, *Macromolecules*, 1996, **29**, 5368–5374.
41 A. Penman and G. Sanderso, *Carbohydr. Res.*, 1972, **25**, 273–282.
42 H. H. Winter, *Polym. Eng. Sci.*, 1987, **27**, 1698.
43 H. H. Winter and F. Chambon, *J. Rheol.*, 1986, **30**, 367–382.
44 F. Chambon and H. H. Winter, *Polym. Bull.*, 1985, **13**, 499–503.
45 A. Ponton, S. Barboux-Doeuff and C. Sanchez, *Colloids Surf., A*, 2000, **162**, 177–192.
46 F. Chambon, Z. S. Petrovic, W. J. Macknight and H. H. Winter, *Macromolecules*, 1986, **19**, 2146–2149.
47 F. Chambon and H. H. Winter, *J. Rheol.*, 1987, **31**, 683–697.
48 A. K. Higham, L. A. Garber, D. C. Latshaw II, C. K. Hall, J. A. Pojman and S. A. Khan, *Macromolecules*, 2014, **47**, 821–829.
49 M. Golmohamadi and K. J. Wilkinson, *Carbohydr. Polym.*, 2013, **94**, 82–87.
50 V. Normand, S. Muller, J.-C. Ravey and A. Parker, *Macromolecules*, 2000, **33**, 1063–1071.
51 S. Nemir and J. L. West, *Ann. Biomed. Eng.*, 2010, **38**, 2–20.
52 G. Skjakbraek, O. Smidsrod and B. Larsen, *Int. J. Biol. Macromol.*, 1986, **8**, 330–336.
53 V. Morris, A. Tsiami and G. J. Brownsey, *J. Carbohydr. Chem.*, 1995, **14**, 667–675.

Supplemental Information

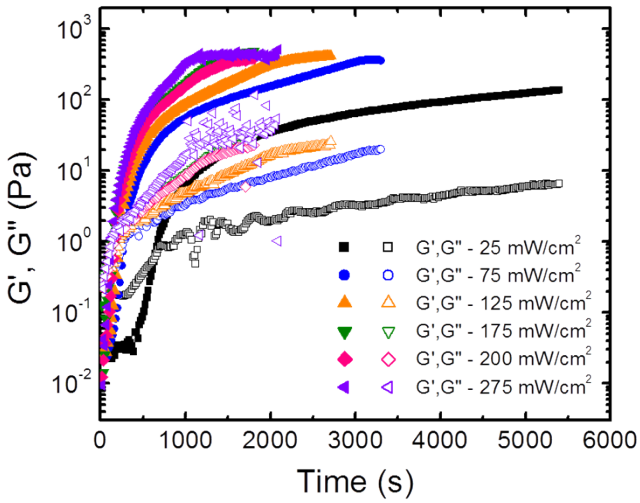

Supplemental Figure 1. Time sweeps of 4 wt./vol.% alginate, 60 mM PAG, and 30 mM $CaCO_3$ exposed to UV irradiation at varying intensities. The G'-G" crossover is delayed as the irradiation intensity decreases.

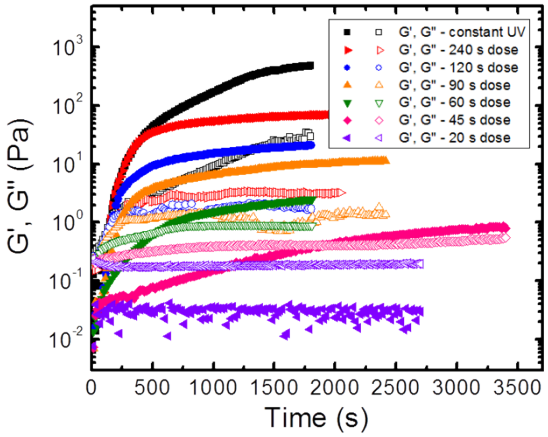

Supplemental Figure 2. Time sweeps of 4 wt./vol.% alginate, 60 mM PAG, and 30 mM $CaCO_3$subjected to UV irradiation for varying durations of exposure.

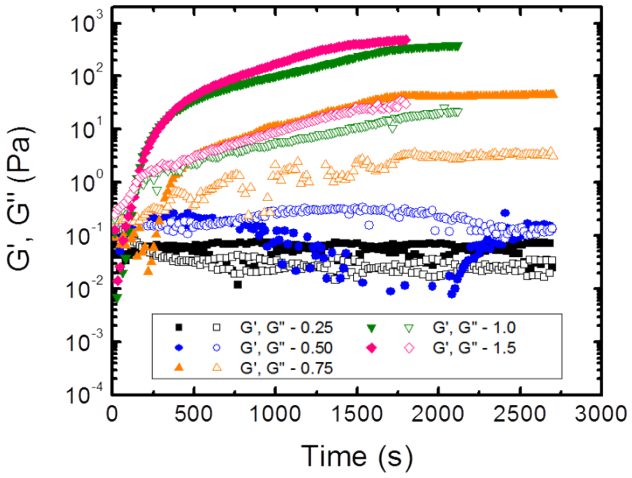

Supplemental Figure 3. Time sweeps monitoring G' and G" over time for 4 wt./vol.% alginate containing varying concentrations of $CaCO_3$ when exposed to UV irradiation.